


# High-Temperature Superconductor Coatings for Beam Impedance Reduction in Particle Colliders: Nonlinear Effects

Sergio Calatroni , *Member, IEEE*, and Ruggero Vaglio

**Abstract**—Coating of surfaces facing particle beams with high-temperature superconductors (HTS) for reducing the beam coupling impedance is being considered for the next generation of hadron colliders, such as the FCC-hh at CERN, where HTS would be exposed to the high-frequency wakefields generated by the particle bunches and to the strong field of the steering magnets. In this frame, we present a simple model for the calculation of the microwave response of HTS exposed to a strong external magnetic field, which takes into account the nonlinearity of the pinning potential of the vortex lattice. The equation of motion of the vortex lattice is solved in first-order approximation, and we calculate the amplitude of the third-harmonic components in the electric field produced by vortex oscillation. We deduce the time-dependent surface impedance, which could serve as a boundary condition in the simulation codes for the calculation of beam-stability phenomena in particle accelerators. Finally, time-integration of the surface impedance allows exploring the dependence of the surface impedance on surface currents, useful for analyzing the experimental results obtained using simple resonators in terms of our model.

**Index Terms**—Accelerators, high-temperature superconductors (HTS), impedance, nonlinearities, surface impedance.

## I. INTRODUCTION

SEVERAL new applications of high-temperature superconductors (HTS) have been discussed in the scientific literature in recent years, requiring operation of HTS at high frequency and in presence of a strong magnetic field. One notable example is the case for beam coupling impedance reduction in future particle colliders, such as the FCC-hh at CERN [1] or CPPC in China [2], where the high-frequency image currents produced by the beam would flow on the inner surface of a screen, coated with HTS, lining the inside of the magnets which steer the beam. The assessment of the potential performance and of optimal material parameters [3] and the possible choices for the most adequate manufacturing technologies for the application of

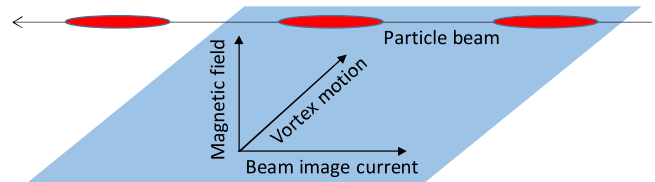


Fig. 1. Schematic electromagnetic configuration: The motion of the vortices created by the external magnetic field is in the plane of the superconductor's surface, perpendicular to both the beam image current and the external field.

HTS on the FCC-hh beam screen have been already extensively discussed [4], [5]. HTS could also play a significant role in next-generation detectors for the hypothetical axion particles, where a virtual photon from a strong static magnetic field is converted by the axion into a real radiofrequency (RF) photon inside a high-quality factor resonant cavity [6], [7]. The use of HTS is also considered for the muon capture and cooling cavities for a possible future muon collider [8]. In all cases, optimization of the surface impedance in presence of a strong magnetic field is a key enabler.

HTS have an intrinsic nonlinear behavior in RF as a function of the intensity of surface currents, a phenomenon which is extensively discussed in the literature and intimately related to d-wave pair-breaking [9]–[12]. Extrinsic effects, such as uniform heating [13], Josephson-junction-like weak links at grain boundaries [14], [15] and trapped RF vortices in weak links [16], all typically related to the HTS quality [17], also play a role in some circumstances and are source of nonlinearities.

A nonlinear behavior of the surface impedance can also be expected in the presence of a strong magnetic field, and it is indeed observed experimentally [18], [19] to dominate the other contributions mentioned above. Among the possible causes of this latter effect lies the nonlinearity of the vortex lattice pinning potential. The aim of this article is to make an explicit model of nonlinearities suitable for assessing their effect on beam coupling impedance in particle accelerators, with a focus on the FCC-hh. An illustration of the electromagnetic configuration in particle accelerators is given in Fig. 1, to help establishing the link with the theoretical models described below.

Vortex dissipation under RF drive has been investigated for many decades. Under the assumptions of a rigid vortex lattice and of uniform RF currents across the thickness of the superconductor, as in a thin slab, Gittleman and Rosenblum (GR) described the dissipation of the rigid flux lattice as in a

Manuscript received December 4, 2020; revised January 12, 2021; accepted January 18, 2021. Date of publication January 21, 2021; date of current version February 18, 2021. This article was recommended for publication by Associate Editor Anna Kario. (*Corresponding author: Sergio Calatroni.*)

Sergio Calatroni is with the CERN, 1211 Geneva, Switzerland (e-mail: sergio.calatroni@cern.ch).

Ruggero Vaglio is with the Dipartimento di Fisica, Università di Napoli Federico II, CNR-SPIN and INFN, 80131 Napoli, Italy (e-mail: ruggero.vaglio@na.infn.it).

Color versions of one or more figures in this article are available at <https://doi.org/10.1109/TASC.2021.3053299>.

Digital Object Identifier 10.1109/TASC.2021.3053299

forced linear oscillator [20]. The model has been extended by several authors, including, for example, vortex creep [21], or the elasticity of the vortex lattice in collective pinning models [22], [23]. For a large density of pinning centers, the GR model is equivalent to a summation over individual vortices having identical pinning potentials. The GR theoretical framework can then be used for the study of single-vortex dynamics, further including vortex line tension and Larkin-Ovchinnikov instabilities [24], or the expected exponential decrease of surface currents inside the superconductor [25]. A different approach to take into account the penetration depth of surface currents has been developed in the frame of the classical rigid-vortex-lattice GR model in [26] and [27] by calculating the complex effective resistivity  $\rho_{eff}$  considering the vortex lattice contribution and then the surface impedance, using the classical formula  $Z_{sf} = (1 + i)\sqrt{\frac{\mu_0\omega}{2}}\rho_{eff}$  (where  $\omega$  is the angular frequency of the RF field), which holds for a thick slab or for a bulk material in the case of a local current-field relation  $E = \rho_{eff}J$ . The effective resistivity  $\rho_{eff}$  can then be extended to include vortex creep and nonlocal pinning effects [28].

The GR model, in its single-vortex formulation, has been extended in a rather straightforward way to the case of a nonlinear pinning potential, as discussed in [29] for the case of low-temperature superconductors at low magnetic field. In this article, following [29], we develop a simple model based on the single-vortex GR approach and we introduce a nonlinear pinning potential for vortices in HTS. Several experiments on HTS justify this simple approach that neglects vortex creep and nonlocal pinning effects, valid for REBCO in the presence of a large density of pinning centers [30], [28], such as modern coated conductors (CC) with artificial pinning centers [31], which are the most mature material candidates for lining the FCC-hh beam screen [5].

We will solve the oscillator equation for the vortex lattice motion at the first order in the perturbation introduced by the nonlinearities, both in the simple case of uniform RF current density across the thickness of the superconductor (thin slab), and taking into account the decrease of surface currents inside the superconductor (thick slab or bulk superconductor). The model predicts the generation of odd harmonics, which could have an impact on beam stability in the case of the FCC-hh, and we will write explicit equations for the surface impedance which could serve as boundary conditions in beam dynamics simulation codes for evaluating the wakefields generated by the particle bunches, and their effect on instabilities [32]. The obtained results are analyzed for frequencies and amplitudes, which are compatible with the FCC-hh beam parameters and with the experiments on small HTS samples performed in the context of the FCC-hh study.

## II. VORTEX ARRAY EQUATION OF MOTION IN HTS USING A REALISTIC, NONQUADRATIC POTENTIAL

The original GR model considers an applied dc field  $B_0$  perpendicular to a thin superconducting slab, with the vortex lattice behaving like a rigid array. This is mathematically equivalent to the equation for single flux lines individually pinned, where

$B_0 = n\phi_0$  is the external field,  $n$  is the number of fluxons per unit surface penetrating the sample, and  $\phi_0$  is the flux quantum. The driving RF current, perpendicular to the dc field, is assumed to be uniform along the slab thickness  $d$ . For small displacements of the flux lines (small applied RF current compared to the critical current), it is reasonable to assume an harmonic potential,  $U(x) = \frac{1}{2}kx^2$ , generating a linear force per unit length  $-kx$ , where  $x$  is the displacement from the equilibrium position along the RF current direction. This results in the GR equation of motion for the flux:

$$\eta\dot{x}(t) + kx(t) = \varphi_0 J_{rf0} \cos \omega t. \quad (1)$$

Here,  $\eta = \varphi_0 B_{c2} / \rho_n$  is the flow viscosity per unit length,  $B_{c2}$  the superconductor upper critical field, and  $\rho_n$  the normal-state electrical resistivity,  $J_{rf0}$  is the maximum amplitude of the RF current of angular frequency  $\omega$  ( $\varphi_0 J_{rf0}$  is the maximum force per unit length exerted by the RF field on a flux line). The effective mass per unit length  $m$  of the fluxons is small and the acceleration term  $m\ddot{x}(t)$  is thus neglected.

In the case of type-II superconductors, a realistic potential describing the flux motion around the equilibrium position has been calculated from the Ginzburg–Landau (GL) equations [33], and is given by

$$U(x) = -\frac{U_0}{1 + (x/\xi_v)^2} \quad (2)$$

where  $\xi_v$  ranges from  $\xi_v \cong \xi$  to  $\xi_v \cong \sqrt{2}\xi$  depending on the GL parameter  $\kappa$ . It has been shown experimentally that this potential correctly describes the pinning of vortices on dislocations in HTS [34].

Introducing the form (2) for the potential, the GR equation of motion (1) becomes

$$\eta\dot{x}(t) + k \frac{x(t)}{\left[1 + (x(t)/\xi_v)^2\right]^2} = \phi_0 J_{rf0} \cos \omega t \quad (3)$$

with  $k = 2U_0/\xi_v^2$  and the dot indicates the time derivative. The RF electric field amplitude, neglecting the term due to the intrinsic HTS superconductor complex resistivity (much smaller than the Lorentz field generated by the vortex lattice oscillations in high magnetic fields), is then given by  $E_{rf} = B_0\dot{x}$ . It is also easy to show that (3) is functionally very similar to (10) of [29] when  $\gamma = 0.75k/\xi_v$ .

Particle bunches in an accelerator induce image currents on the beam facing surfaces with a time-varying profile, and a resulting wide-band frequency spectrum [4]. The time-domain current profile of the bunch  $J_{rf0}f(t)$  could in practice replace the single mode oscillatory driving term  $J_{rf0} \cos \omega t$  in (3). Equation (3) thus modified could then in principle be inserted in beam dynamics numerical simulation codes and would be fully sufficient for evaluating the effect of HTS nonlinearities on particle beam stability [32], through the calculation of  $E_{rf}$  and of its effect back on the beam itself.

It is nevertheless useful for a better physics insight to analyze the single mode  $\omega$  behavior, and it is easy to show that the generated EM field contains a large component at the same frequency of the forcing RF current, and odd harmonics whose

amplitude increases for increasing amplitude of the forcing term, the main contribution given by the third harmonic signal. For this purpose, it is convenient to rewrite (3) in adimensional units, introducing the following adimensional parameters:  $y = x/\xi_v$ ,  $\tau = \omega t$ ,  $a_{rf} = \phi_o J_{\text{rf}o}/k\xi_v$ ,  $r = \omega/\omega_o$ , where  $\omega_o = k/\eta$  is the depinning frequency, a key parameter characterizing the RF behavior of the vortex lattice. Since the superconductor critical current in the vortex state is proportional to the pinning force constant per unit length  $k$ , it follows that  $a_{rf}$  is proportional to the ratio between the maximum RF current and the critical current.

In these units, (3) becomes

$$r\dot{y}(\tau) + \frac{y(\tau)}{[1 + y(\tau)^2]^2} = a_{rf} \cos \tau \quad (4)$$

where the dot now indicates derivative with respect to  $\tau$ . Equation (4) can be easily solved numerically. In these units,  $E_{rf} = \omega\xi_v B_o \dot{y}(\tau)$ .

The nonlinear equation (4) can be also solved analytically by perturbation methods. One can first develop in Taylor series the adimensional nonlinear term in (4), derived from the potential described by (2)

$$\frac{y(\tau)}{[1 + y(\tau)^2]^2} = y(\tau) - 2y^3(\tau) + O(y^5). \quad (5)$$

This leads to the equation

$$r\dot{y}(\tau) + y(\tau) = a_{rf} \cos \tau + 2y^3(\tau) - O(y^5). \quad (6)$$

Then, we assume  $y(\tau) = y_o(\tau) + y_1(\tau)$  with  $y_1 \ll y_o$ . By substitution in (6), neglecting all second-order terms (or higher), we come to the following set of linear differential equations:

$$r\dot{y}_o(\tau) + y_o(\tau) = a_{rf} \cos \tau \quad (7a)$$

$$r\dot{y}_1(\tau) + y_1(\tau) = 2y_o^3(\tau). \quad (7b)$$

Equation (7a) represents the linear GR equation in adimensional units and is easily solved giving

$$y_o(\tau) = \frac{a_{rf}}{\sqrt{1+r^2}} \cos(\tau - \phi) \quad (8a)$$

$$\dot{y}_o(\tau) = -\frac{a_{rf}}{\sqrt{1+r^2}} \sin(\tau - \phi) \quad (8b)$$

with  $\phi = tg^{-1}r$  (we note that  $\frac{1}{\sqrt{1+r^2}} = \cos \varphi$ ).

The solution of (7a), given by (8a) and (8b), is fully equivalent to the GR solution, which is given in complex notation in [20].

By substituting the expression for  $y_o(\tau)$  given by (8a) into (7b), after simple, but tedious, calculations (see Appendix A), we are led to the following closed form for the perturbative velocity term  $\dot{y}_1(\tau)$ :

$$\dot{y}_1(\tau) = -\frac{3a_{rf}^3}{2(1+r^2)^2} \times \left[ \sin(\tau - 2\phi) + \sqrt{\frac{1+r^2}{1+9r^2}} \sin(3\tau - 3\phi - tg^{-1}3r) \right]. \quad (9)$$

Finally, the generated electric field, at the first order, is given by

$$E_{rf}(\tau) = \omega\xi_v B_o [\dot{y}_o(\tau) + \dot{y}_1(\tau)] \quad (10)$$

with  $\dot{y}_o(\tau)$  and  $\dot{y}_1(\tau)$  given, respectively, by (8b) and (9). From the latter, it is clear that  $E_{rf}$  presents a significant third order ( $3\omega$ ) component, whose amplitude scales with  $a_{rf}^3$ . The main first order component, given by (8b), scales as  $a_{rf}$ , so that the ratio between third and first harmonic signal scales approximately as  $a_{rf}^2$ . We note that an out-of-phase first order component which scales with  $a_{rf}^3$  is also present in  $\dot{y}_1(\tau)$ . To conclude, we note comparing (8b) and (9) that the relative amplitude of  $\dot{y}_1(\tau)$  with respect to  $\dot{y}_o(\tau)$  decreases with increasing  $r$ .

In Fig. 2 we compare the value of  $\dot{y}_1(\tau)$  calculated from (9), with the equivalent term  $\dot{y}(\tau) - \dot{y}_o(\tau)$  calculated numerically. The numerical solution is performed from an initial condition  $y(0) = 0$ , while the results are displayed starting after about five full cycles, to allow stabilizing any initial out-of-equilibrium movement. The results are displayed for  $r = 0.1$  and  $r = 0.5$ . These values have been chosen because they correspond respectively to the maximum frequency of the FCC-hh bunch spectrum (about 1.5 GHz [4]) and to the typical frequency at which small samples of CC are characterized within the FCC-hh study (8 GHz [5]), relative to realistic values of the depinning frequency of HTS (15–25 GHz depending on the CC provider [35]). The numerical and analytical solutions are practically superposed, except at higher driving amplitude  $a_{rf}$ . A detailed numerical analysis allows us to verify that the necessary condition for the perturbative solution  $y_1 \ll y_o$  is always satisfied for  $a_{rf} < 0.25$ . The surface current equivalent to this value of  $a_{rf}$  is well above the peak surface current expected in the FCC-hh, estimated at about  $250 \text{ Am}^{-1}$  per width of the CC lining the beam screen [4], to be compared with the critical currents measured on the HTS CCs foreseen for this application, which span the range  $10^3$ – $10^4 \text{ Am}^{-1}$ , depending on the CC provider [5].

We note that the fundamental and the third harmonic are clearly distinguishable in Fig. 2, and the substantial equivalence between numerical simulation and first-order solution confirm that the third harmonic component is the dominant high-order term generated by the assumed nonlinear potential.

### III. COMPLEX RESISTIVITY IN THE NONLINEAR CASE

The relation connecting the electric field  $E_{rf}(\tau)$  to the driving current  $J_{rf}(\tau)$  can be written in terms of the Ohm law in complex notation:

$$\tilde{E}_{rf}(\tau) = \tilde{\rho}_{sf}(\tau) \tilde{J}_{rf}(\tau) \quad (11)$$

where  $\tilde{\rho}_{sf}(\tau) = \rho_{sf}^R(\tau) + i\rho_{sf}^I(\tau)$  is a time-dependent, complex resistivity, and  $\tilde{J}_{rf}(\tau) = J_{\text{rf}o} e^{i\tau}$ .

The forcing current used in (3) is given by  $\text{Re}[\tilde{J}_{rf}(\tau)] = J_{\text{rf}o} \cos \tau$  so that  $\text{Re}[\tilde{E}_{rf}(\tau)]$  should reproduce  $E_{rf}(\tau)$  as given

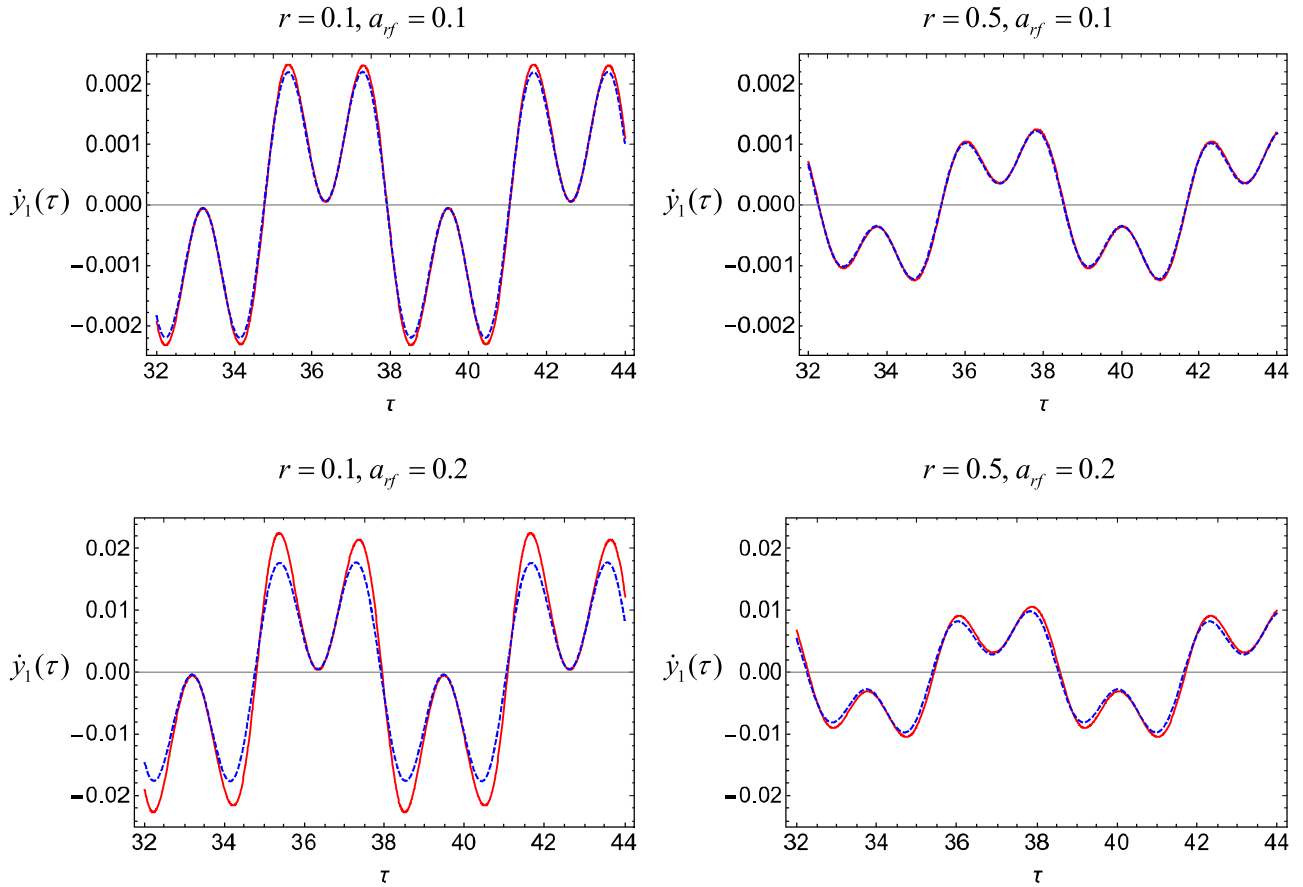


Fig. 2. Numeric solution of (4) (red) compared to its analytic first-order solution (9) (blue, dashed) as discussed in the text, for the different values of  $r$  and  $a_{rf}$  shown in the captions.

by (10), (8b), and (9). This is achieved through

$$\rho_{sf}^R(\tau) = \rho_{sfo}^R \times \left\{ 1 + \frac{3a_{rf}^2}{2r(1+r^2)} \left[ \frac{2r}{1+r^2} - \sqrt{\frac{1+r^2}{1+9r^2}} \sin(4\tau - \delta) \right] \right\} \quad (12a)$$

$$\rho_{sf}^I(\tau) = \rho_{sfo}^I \times \left\{ 1 + \frac{3a_{rf}^2}{2(1+r^2)} \left[ \frac{1-r^2}{1+r^2} - \sqrt{\frac{1+r^2}{1+9r^2}} \cos(4\tau - \delta) \right] \right\} \quad (12b)$$

where  $\delta = 3tg^{-1}r + tg^{-1}3r$  and

$$\begin{aligned} \tilde{\rho}_{sfo} &= \rho_{sfo}^R + i\rho_{sfo}^I = \rho_n \frac{B_o}{B_{c2}} \left( \frac{r^2}{1+r^2} + i \frac{r}{1+r^2} \right) \\ &= \rho_n \frac{B_o}{B_{c2}} (\alpha + i\beta) \end{aligned} \quad (13)$$

is the zero RF field value of the complex resistivity, i.e., the complex resistivity in the linear GR model [3]. The deduction of (12) is reported in Appendix B.

The time-dependent surface impedance in the approximation of uniform RF current along a thin slab of thickness  $d$  is simply given by

$$Z_{sf}(\tau) = R_{sf}(\tau) + iX_{sf}(\tau) = \frac{\rho_{sf}^R(\tau)}{d} + i \frac{\rho_{sf}^I(\tau)}{d}. \quad (14)$$

The zero RF field surface impedance is, obviously:  $Z_{sfo} =$

$$R_{sfo} + iX_{sfo} = \frac{\rho_{sfo}^R}{d} + i \frac{\rho_{sfo}^I}{d}.$$

It is possible, for a thin slab, to calculate the RF current dependence of the surface impedance. The quantities which are experimentally measured can be derived from (12) and (14) are

$$\bar{R}_{sf} = \frac{1}{2\pi} \int_0^{2\pi} R_{sf}(\tau) d\tau = R_{sfo} \left[ 1 + \frac{3a_{rf}^2}{(1+r^2)^2} \right] = R_{sfo} a \quad (15a)$$

$$\begin{aligned} \bar{X}_{sf} &= \frac{1}{2\pi} \int_0^{2\pi} X_{sf}(\tau) d\tau \\ &= X_{sfo} \left[ 1 + \frac{3a_{rf}^2}{2} \frac{(1-r^2)}{(1+r^2)^2} \right] = X_{sfo} b. \end{aligned} \quad (15b)$$

An alternative method to calculate the RF current amplitude-dependent average surface resistance is through the calculation of the average dissipated power, using the method reported in [29]. It can be shown that the two methods give identical results (at the first order).

It is worth noting that (14) and (15) hold for a “suspended” thin superconducting film (e.g., deposited on a dielectric substrate) and would not apply for a thin film deposited on a metallic substrate, as in the case of the HTS coated beam screen in particle colliders.

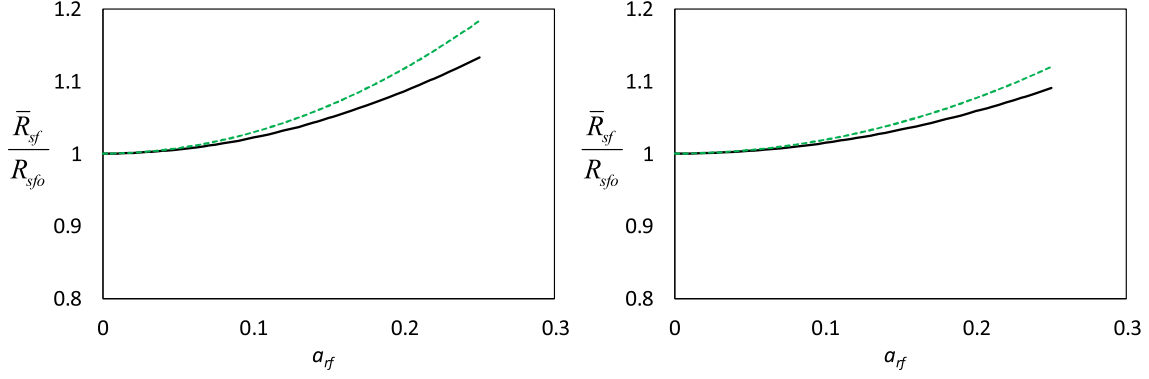


Fig. 3. Dependence of  $\frac{\bar{R}_{sf}}{R_{sfo}}$  on  $a_{rf}$  following (14) (green, dashed) and (18a) (black), for  $r = 0.1$  (left) and  $r = 0.5$  (right).

#### IV. SURFACE IMPEDANCE IN A THICK FILM

As discussed in Section I, we can calculate the surface impedance for a thick film (or for a bulk) considering the current-field relation given by (11), with the resistivity given by (12) and (13), and the classical formula for the surface impedance derived from the Maxwell equations. Writing  $\tilde{\rho}_{sf}(\tau) = \tilde{\rho}_{csf} + \tilde{\rho}_{vsf}(\tau)$  and since for  $a_{rf} \ll 1$  the time dependent part  $\tilde{\rho}_{vsf}(\tau)$  of  $\tilde{\rho}_{sf}(\tau)$  is small with respect to the time independent part  $\tilde{\rho}_{csf}$  we can consider the following approximations:

$$Z_{sf}(\tau) \cong (1+i)\sqrt{\frac{\mu_0\omega\tilde{\rho}_{sf}(\tau)}{2}} \cong (1+i)\sqrt{\frac{\mu_0\omega\tilde{\rho}_{csf}}{2}} \times \left(1 + \frac{\tilde{\rho}_{vsf}(\tau)}{2\tilde{\rho}_{csf}}\right) = Z_{csf} \left(1 + \frac{\tilde{\rho}_{vsf}(\tau)}{2\tilde{\rho}_{csf}}\right). \quad (16)$$

It is easy to show that (16) reproduces (14) in the case of a thin film [36].

After some simple calculation extracting  $\tilde{\rho}_{vsf}(\tau)$  and  $\tilde{\rho}_{csf}$  from (12), (16) leads to the real and imaginary parts of the surface impedance  $Z_{sf}(\tau)$ . This approach, developed in Appendix C, is particularly relevant for thick films, and reproduces the square root dependence of the average surface resistance on the applied magnetic field observed in experiments pertinent to this study [5], [35], all contained in the time-independent term  $Z_{csf}$ . The surface resistance deduced from (12) to (14) implies instead a linear dependence, which is typically observed for thin films [37], [38].

We can finally write the time-averaged surface impedance in this approach, noting that  $\frac{1}{2\pi} \int_0^{2\pi} \tilde{\rho}_{vsf}(\tau) d\tau = 0$  and thus, with reference to (16) we obtain

$$\bar{Z}_{sf} = \frac{1}{2\pi} \int_0^{2\pi} Z_{sf}(\tau) d\tau \cong Z_{csf} = R_{csf} + iX_{csf}. \quad (17)$$

The expressions for  $R_{csf}$  and  $X_{csf}$  are deduced in Appendix C

$$R_{csf} = R_n \sqrt{\frac{B_o}{B_{c2}}} \sqrt{\sqrt{(\alpha a)^2 + (\beta b)^2} - \beta b} \quad (18a)$$

$$X_{csf} = X_n \sqrt{\frac{B_o}{B_{c2}}} \sqrt{\sqrt{(\alpha a)^2 + (\beta b)^2} + \beta b}. \quad (18b)$$

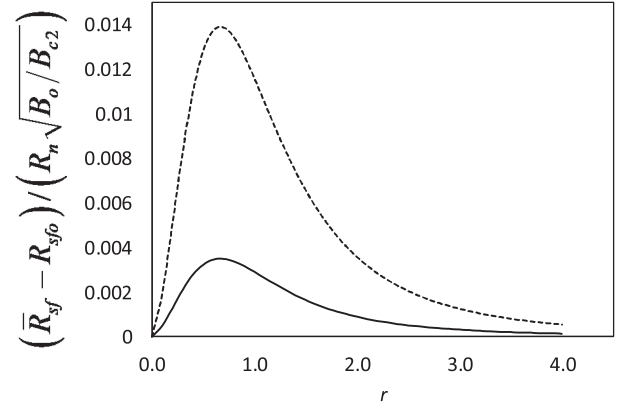


Fig. 4. Dependence of  $(\bar{R}_{sf} - R_{sfo}) / (R_n \sqrt{B_o/B_{c2}})$  on  $r$  from (18a), for  $a_{rf} = 0.1$  (solid line) and  $a_{rf} = 0.2$  (dashed).

Here,  $R_n = X_n = \sqrt{\frac{\mu_0\rho_n\omega}{2}}$  are the real and imaginary parts of the surface impedance in the normal state and  $\alpha, \beta, a, b$  already defined (13), (15).

The calculated values for the real and imaginary part of the time-dependent surface impedance could be used in 2-D beam coupling impedance simulation codes as boundary conditions for calculating the wakefields generated by the particle bunches, readily showing the possible impact of any third harmonic component [32].

In Fig. 3, we compare the dependence of the ratio  $\bar{R}_{sf}/R_{sfo}$  on the magnitude of the RF currents  $a_{rf}$  from both (14) (thin film) and (18a) (thick film - bulk), plotted for  $r = 0.1$  and  $r = 0.5$ . The surface resistance obviously increases with the magnitude of the RF currents.

The  $r$  dependence is illustrated in Fig. 4, where we compare the difference  $(\bar{R}_{sf} - R_{sfo})$  normalized to  $R_n \sqrt{B_o/B_{c2}}$  from (18a), for  $a_{rf} = 0.1$  and  $a_{rf} = 0.2$ .

In Fig. 5, we show the dependence of the ratio  $\bar{X}_{sf}/X_{sfo}$  on the magnitude of the RF current  $a_{rf}$  from (18b), for  $r = 0.1$  and  $r = 0.5$ , which of course also increases with the amplitude of the RF current, at a different rate depending on the normalized frequency  $r$ .

We note that in general the RF field penetration depth is proportional to the imaginary part of the surface impedance

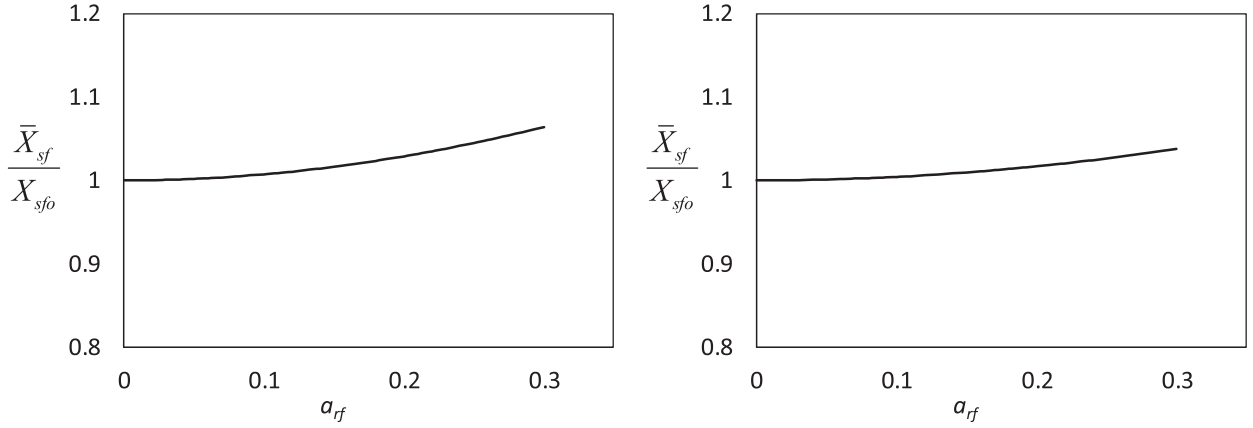


Fig. 5. Dependence of  $\frac{\bar{X}_{sf}}{X_{sfo}}$  on  $a_{rf}$  following (18b), for  $r = 0.1$  (left) and  $r = 0.5$  (right).

[21]  $\lambda_s = \frac{X_s}{\mu_o \omega}$  such that, in the limit  $r \ll 1$ , we obtain the simple form  $\lambda_{sfo} = \frac{X_{sfo}}{\mu_o \omega} = \delta_n \sqrt{r} \sqrt{\frac{B_o}{B_{c2}}}$ , where  $\delta_n = \sqrt{\frac{2\rho_n}{\mu_o \omega}}$  is the normal state penetration depth. It is worth observing that to quantitatively compare the experimental data with our theoretical formulas in the case of thick films the condition  $d \geq \lambda_{sfo}$  must be satisfied.

Finally, we note that in the practical case of a future HTS coated beam screen, the thickness of the coating might not be enough to guarantee the validity of the bulk approximation. In that case, a more complex modeling, taking into account the presence of the metallic substrate beneath the HTS, should be developed.

## V. CONCLUSION

In this article we have discussed a model, which provides a closed formula for the first-order analytic solution of the equation of motion of the rigid vortex lattice of HTS under microwave excitation in a strong magnetic field. The solution allows calculating analytical formulas for the time-dependent nonlinear surface impedance and the amplitude of the third harmonic signal generated by the nonlinearities. The results are successfully compared with numerical solutions, showing generally a good equivalence. We discuss also different approximations for the time-averaged surface resistance and reactance, as a function of the RF amplitude.

The model results have been specifically formulated in order to allow their use in beam-dynamics stability codes. The calculated values for the real and imaginary part of the time-dependent surface impedance could in fact be used as boundary conditions for the wakefields generated by the particle bunches, in order to allow proper simulation of the effects of the harmonics, in the case of the HTS coated beam screen as foreseen by the FCC-hh study at CERN.

The model predictions can in principle be verified by ad hoc experiments, analyzing the effect of the harmonics in terms of their global effect on the surface resistance of small samples. In particular, the simultaneous measure of the depinning frequency, using techniques such as the Corbino disk [36], [39], and of the

RF current dependence of the surface resistance could allow a self-consistent estimation of the amplitude of the generated third harmonic signal, which is more difficult to measure directly.

## APPENDIX A

We start from (7b), with  $y_o$  given by (8a)

$$r\dot{y}_1(\tau) + y_1(\tau) = \frac{2a_{rf}^3}{(1+r^2)^{3/2}} \cos^3(\tau - \phi). \quad (A1)$$

Given the equivalence  $\cos^3(\tau - \phi) = \frac{3}{4} \cos(\tau - \phi) + \frac{1}{4} \cos 3(\tau - \phi)$ , (A1) can be split in two equivalent equations:

$$r\dot{y}_{11}(\tau) + y_{11}(\tau) = \frac{3a_{rf}^3}{2(1+r^2)^{3/2}} \cos(\tau - \phi) \quad (A2a)$$

$$r\dot{y}_{13}(\tau) + y_{13}(\tau) = \frac{a_{rf}^3}{2(1+r^2)^{3/2}} \cos 3(\tau - \phi) \quad (A2b)$$

with

$$y_1(\tau) = y_{11}(\tau) + y_{13}(\tau). \quad (A3)$$

We look for solutions of the form

$$y_{11}(\tau) = Y_{11} \cos[(\tau - \phi) - \varphi_{11}] \quad (A4a)$$

$$y_{13}(\tau) = Y_{13} \cos[3(\tau - \phi) - \varphi_{13}]. \quad (A4b)$$

After substitution in (A2), it is straightforward to obtain

$$\phi_{11} = tg^{-1}r = \varphi, \quad Y_{11} = \frac{3a_{rf}^3}{2(1+r^2)^2} \quad (A5a)$$

$$\phi_{13} = tg^{-1}3r, \quad Y_{13} = \frac{a_{rf}^3}{2(1+r^2)^{3/2} \sqrt{1+9r^2}}. \quad (A5b)$$

Further substitution of (A5) in (A4) and then in (A3) and finally taking the time derivative leads to (9).

## APPENDIX B

Using the already introduced relations:  $a_{rf} = \varphi_o J_{rf0}/k\xi_v$ ,  $r = \omega/\omega_o$ ,  $\omega_o = k/\eta$  and  $\eta = \varphi_o B_{c2}/\rho_n$  it is  $J_{rf0} \rho_n \frac{B_o}{B_{c2}} r = \omega \xi_v B_o a_{rf}$ .

We can then rewrite (10), (8b), and (9) in the form:

$$E_{rf}^R(\tau) = -J_{rfo}\rho_n \frac{B_o}{B_{c2}} r \left\{ \frac{\sin(\tau - \phi)}{\sqrt{1+r^2}} + \frac{3a_{rf}^2}{2(1+r^2)^2} \times \left[ \sin(\tau - 2\phi) + \sqrt{\frac{1+r^2}{1+9r^2}} \sin(3\tau - 3\phi - tg^{-1}3r) \right] \right\}. \quad (B1a)$$

This represents the real part of the complex electric field function defined by (11).

The imaginary part can be obtained by using in (4) a forcing term given by  $a_{rf} \sin \tau$ , following the same route that lead to (10). This leads to

$$E_{rf}^I(\tau) = J_{rfo}\rho_n \frac{B_o}{B_{c2}} r \left\{ \frac{\cos(\tau - \phi)}{\sqrt{1+r^2}} + \frac{3a_{rf}^2}{2(1+r^2)^2} \times \left[ \cos(\tau - 2\phi) - \sqrt{\frac{1+r^2}{1+9r^2}} \cos(3\tau - 3\phi - tg^{-1}3r) \right] \right\}. \quad (B1b)$$

Using (B1), the electric field in complex notation is given by

$$\tilde{E}_{rf}(\tau) = iJ_{rfo}\rho_n \frac{B_o}{B_{c2}} r \left\{ \frac{e^{i(\tau-\phi)}}{\sqrt{1+r^2}} + \frac{3a_{rf}^2}{2(1+r^2)^2} \times \left[ e^{i(\tau-2\phi)} - \sqrt{\frac{1+r^2}{1+9r^2}} e^{-i(3\tau-3\phi-tg^{-1}3r)} \right] \right\}. \quad (B2)$$

Inserting (B2) in (11), considering that  $\tilde{J}_{rf}(\tau) = J_{rfo}e^{i\tau}$  we can deduce the complex resistivity

$$\tilde{\rho}_{sf}(\tau) = i\rho_n \frac{B_o}{B_{c2}} r \left\{ \frac{e^{-i\phi}}{\sqrt{1+r^2}} + \frac{3a_{rf}^2}{2(1+r^2)^2} \times \left[ e^{-i2\phi} - \sqrt{\frac{1+r^2}{1+9r^2}} e^{-i(4\tau-3\phi-tg^{-1}3r)} \right] \right\}. \quad (B3)$$

Using (13), remembering that  $\phi = tg^{-1}r$  and using trivial trigonometrical relations we obtain

$$\rho_{sf}^R(\tau) = \rho_{sfo}^R \left\{ 1 + \frac{3a_{rf}^2}{2r(1+r^2)} \times \left[ \sin 2\phi - \sqrt{\frac{1+r^2}{1+9r^2}} \sin(4\tau - 3\phi - tg^{-1}3r) \right] \right\} \quad (B4a)$$

$$\rho_{sf}^I(\tau) = \rho_{sfo}^I \left\{ 1 + \frac{3a_{rf}^2}{2(1+r^2)} \times \left[ \cos 2\phi - \sqrt{\frac{1+r^2}{1+9r^2}} \cos(4\tau - 3\phi - tg^{-1}3r) \right] \right\}. \quad (B4b)$$

Defining  $\delta = 3tg^{-1}r + tg^{-1}3r$  and considering that  $\sin 2\varphi = \frac{2r}{1+r^2}$  and  $\cos 2\varphi = \frac{1-r^2}{1+r^2}$  we are easily led to (12).

## APPENDIX C

Using (13) and recalling that  $\tilde{\rho}_{sf}(\tau) = \rho_{sf}^R(\tau) + i\rho_{sf}^I(\tau)$ , from (12) we can write  $\tilde{\rho}_{sf}(\tau) = \tilde{\rho}_{csf} + \tilde{\rho}_{vsf}(\tau)$  with  $\tilde{\rho}_{csf} = \rho_{csf}^R + i\rho_{csf}^I$ :

$$\rho_{csf}^R = \rho_n \frac{B_o}{B_{c2}} \alpha a \quad (C1a)$$

$$\rho_{csf}^I = \rho_n \frac{B_o}{B_{c2}} \beta b. \quad (C1b)$$

And with  $\tilde{\rho}_{vsf}(\tau) = \rho_{vsf}^R(\tau) + i\rho_{vsf}^I(\tau)$ :

$$\rho_{vsf}^R(\tau) = -\rho_n \frac{B_o}{B_{c2}} \frac{\alpha}{r} \frac{3a_{rf}^2}{2} \frac{1}{(1+r^2)} \sqrt{\frac{1+r^2}{1+9r^2}} \sin(4\tau - \delta) \quad (C2a)$$

$$\rho_{vsf}^I(\tau) = -\rho_n \frac{B_o}{B_{c2}} \beta \frac{3a_{rf}^2}{2} \frac{1}{(1+r^2)} \sqrt{\frac{1+r^2}{1+9r^2}} \cos(4\tau - \delta). \quad (C2b)$$

Recalling (16) and (17) and following (11) from [3] we can now write  $Z_{csf} = (1+i)\sqrt{\frac{\mu_o\omega\tilde{\rho}_{csf}}{2}} = R_{csf} + iX_{csf}$  with

$$R_{csf} = \sqrt{\frac{\mu_o\omega}{2}} \sqrt{\sqrt{\rho_{csf}^R{}^2 + \rho_{csf}^I{}^2} - \rho_{csf}^I} \quad (C3a)$$

$$X_{csf} = \sqrt{\frac{\mu_o\omega}{2}} \sqrt{\sqrt{\rho_{csf}^R{}^2 + \rho_{csf}^I{}^2} + \rho_{csf}^I}. \quad (C3b)$$

From (C1) and (C3), we easily obtain the real and imaginary part of the time-independent surface impedance reported in the text (18). From (12), (16) and (C1)–(C3), it would also be straightforward to calculate the real and imaginary parts of the time-dependent surface impedance.

It is also immediately apparent inspecting (C1) and (C2) that the term  $\left(1 + \frac{\tilde{\rho}_{vsf}(\tau)}{2\tilde{\rho}_{csf}}\right)$  of (16) does not depend on  $B_o/B_{c2}$

## ACKNOWLEDGMENT

The authors would like to thank Massimo Vaglio (University of Rome ‘‘La Sapienza’’) for many useful discussions and suggestions on the analysis of nonlinear equations, and Giovanni Rumolo and Giovanni Iadarola (CERN) for clarifying the requisites for beam-dynamics simulation.

## REFERENCES

- [1] S. Calatroni, ‘‘HTS coatings for impedance reduction in particle accelerators: Case study for the FCC at CERN,’’ *IEEE Trans. Appl. Supercond.*, vol. 26, no. 3, Apr. 2016, Art. no. 3500204.
- [2] P. Gan *et al.*, ‘‘Design study of an YBCO-coated beam screen for the super proton-proton collider bending magnets,’’ *Rev. Sci. Instrum.*, vol. 89, 2018, Art. no. 045114.
- [3] S. Calatroni and R. Vaglio, ‘‘Surface resistance of superconductors in the presence of a dc magnetic field: Frequency and field intensity limits,’’ *IEEE Trans. Appl. Supercond.*, vol. 27, no. 5, Aug. 2017, Art. no. 3500506.
- [4] S. Calatroni *et al.*, ‘‘Thallium-based high-temperature superconductors for beam impedance mitigation in the future circular collider,’’ *Supercond. Sci. Technol.*, vol. 30, 2017, Art. no. 075002.
- [5] T. Puig *et al.*, ‘‘Coated conductor technology for the beamscreen chamber of future high energy circular colliders,’’ *Supercond. Sci. Technol.*, vol. 32, 2019, Art. no. 094006.

- [6] D. Ahn *et al.*, "Superconducting cavity in a high magnetic field," Accessed: Feb. 1, 2021, [Online]. Available: <https://arxiv.org/abs/2002.08769>
- [7] The RADES Collaboration, "Scalable haloscopes for axion dark matter detection in the 30 $\mu$ eV range with RADES," Accessed: Feb. 1, 2021, [Online]. Available: <https://arxiv.org/abs/2002.07639>
- [8] A. Grudjev, "First thoughts on required RF testing infrastructure," in *Proc. Muon Collider Workshop*, CERN Geneva, 2019. [Online]. Available: <https://indico.cern.ch/event/845054/>
- [9] T. Dahm and D. J. Scalapino, "Theory of microwave intermodulation in a high- $T_c$  superconducting microstrip resonator," *Appl. Phys. Lett.*, vol. 69, pp. 4248–4250, 1996.
- [10] G. Benz, S. Wünsch, T. A. Scherer, M. Neuhaus, and W. Jutzi, "Measured temperature dependence of the intermodulation product of coplanar waveguides with s- and d-wave superconductors," *Physica C*, vol. 356 pp. 122–128, 2001.
- [11] G. Cifariello *et al.*, "Intrinsic nonlinearity probed by intermodulation distortion microwave measurements on high quality MgB<sub>2</sub> thin films," *Appl. Phys. Lett.*, vol. 88, 2006, Art. no. 142510.
- [12] D. E. Oates, S.-H. Park, and G. Koren, "Observation of the nonlinear Meissner effect in YBCO thin films: Evidence for a d-wave order parameter in the bulk of the cuprate superconductors," *Phys. Rev. Lett.*, vol. 93, 2004, Art. no. 197001.
- [13] N. T. Cherpak, A. I. Gubin, A. A. Lavrinovich, and S. A. Vitusevich, "Microwave quenching in DC-biased coplanar waveguide based on YBa<sub>2</sub>Cu<sub>3</sub>O<sub>7- $\delta$</sub>  thin film," *IEEE Trans. Appl. Supercond.*, vol. 26, no. 3, 2016, Art. no. 1501204.
- [14] T. L. Hylton, A. Kapitulnik, M. R. Beasley, J. P. Carini, L. Drabeck, and G. Grüner, "Weakly coupled grain model of high-frequency losses in high  $T_c$  superconducting thin films," *Appl. Phys. Lett.*, vol. 53, 1988, Art. no. 1343.
- [15] C. Attanasio, L. Maritato, and R. Vaglio, "Residual surface resistance of polycrystalline superconductors," *Phys. Rev. B*, vol. 43, 1991 pp. 6128–6131.
- [16] J. Halbritter, "RF residual losses, surface impedance, and granularity in superconducting cuprates," *J. Appl. Phys.*, vol. 68, 1990 pp. 6315–6326.
- [17] M. Hein, *High-Temperature-Superconductor Thin Films At Microwave Frequencies*. Berlin, Germany: Springer, 1999.
- [18] J. R. Powell *et al.*, "The nonlinear surface impedance of YBa<sub>2</sub>Cu<sub>3</sub>O<sub>7- $\delta$</sub>  thin films in zero and large applied fields," *J. Appl. Phys.*, vol. 86, 1999, pp. 2137–2145.
- [19] A. M. Portis, *Electrodynamics of High-Temperature Superconductors*. Singapore: World Scientific, 1992.
- [20] J. I. Gittleman and B. Rosenblum, "Radio-Frequency resistance in the mixed state for subcritical currents," *Phys. Rev. Lett.*, vol. 16, 1966, Art. no. 734.
- [21] M. W. Coffey and J. R. Clem, "Unified theory of effects of vortex pinning and flux creep upon the RF surface impedance of type-II superconductors," *Phys. Rev. Lett.*, vol. 67, pp. 386–389, 1991.
- [22] E. H. Brandt, "Penetration of magnetic ac fields into type-II superconductors," *Phys. Rev. Lett.*, vol. 67, pp. 2219–2222, 1991.
- [23] E. B. Sonin, A. K. Tagantsev, and K. B. Traito, "Two-mode electro-dynamics of superconductors in the mixed state," *Phys. Rev. B*, vol. 46, pp. 5830–5832, 1992.
- [24] A. Gurevich and G. Ciovati, "Dynamics of vortex penetration, jumpwise instabilities, and nonlinear surface resistance of type-II superconductors in strong RF fields," *Phys. Rev. B*, vol. 77, 2008, Art. no. 104501.
- [25] M. Checchin, M. Martinello, A. Grassellino, A. Romanenko, and J. F. Zasadzinski, "Electron mean free path dependence of the vortex surface impedance," *Supercond. Sci. Technol.*, vol. 30, 2017, Art. no. 034003.
- [26] A. M. Portis, K. W. Blazey, K. A. Müller, and J. G. Bednorz, "Microwave magneto-surface impedance of high- $T_c$  superconductors," *Europhys. Lett.*, vol. 5, pp. 467–472, 1988.
- [27] R. Marcon, R. Fastampa, M. Giura, and E. Silva, "Vortex-motion dissipation in high- $T_c$  superconductors at microwave frequencies," *Phys. Rev. B*, vol. 43, 1991, Art. no. 2940.
- [28] N. Pompeo and E. Silva, "Reliable determination of vortex parameters from measurements of the microwave complex resistivity," *Phys. Rev. B*, vol. 78, 2008, Art. no. 094503.
- [29] S. Calatroni and R. Vaglio, "A simple model for the RF field amplitude dependence of the trapped flux sensitivity in superconducting RF cavities," *Phys. Rec. Acc. Beams.*, vol. 22, 2019, Art. no. 022001.
- [30] M. Golosovsky, M. Tsindlekht, and D. Davidov, "High-frequency vortex dynamics in YBa<sub>2</sub>Cu<sub>3</sub>O<sub>7</sub>," *Supercond. Sci. Technol.*, vol. 9, pp. 1–15, 1996.
- [31] E. Bartolomé *et al.*, "Vortex pinning properties at dc and microwave frequencies of YBa<sub>2</sub>Cu<sub>3</sub>O<sub>7-x</sub> films with nanorods and nanoparticles," *Supercond. Sci. Technol.*, vol. 33, 2020, Art. no. 074006.
- [32] G. Rumolo and G. Iadarola, (CERN), Private Communication.
- [33] J. R. Clem, "Simple model for the vortex core in a type II superconductor," *J. Low. Temp. Phys.*, vol. 18, pp. 427–434, 1975.
- [34] É. A. Pashitskiĭ and V. I. Vakaryuk, "Pinning of Abrikosov vortices on dislocations and the critical current in high temperature superconductors," *Low Temp. Phys.*, vol. 28, pp. 11–16, 2002.
- [35] A. Romanov *et al.*, "High frequency response of thick REBCO coated conductors in the framework of the FCC study," *Sci. Rep.*, vol. 10, 2020, Art. no. 12325.
- [36] J. C. Booth, D. H. Wu, and S. M. Anlage, "A broadband method for the measurement of the surface impedance of thin films at microwave frequencies," *Rev. Sci. Instrum.*, vol. 65, pp. 2082–2090, 1994.
- [37] K. Nakagawa *et al.*, "Intrinsic surface resistance of YBCO thin films under DC magnetic field," *IEEE Trans. Appl. Supercond.*, vol. 21, no. 3, pp. 587–590, Jun. 2011.
- [38] T. Honma *et al.*, "Microwave surface resistance of YBCO superconducting thin films under high DC magnetic field," *Physica C, Supercond.*, vol. 484, pp. 46–48, 2013.
- [39] E. Silva, N. Pompeo, K. Torokhtii, and S. Sarti, "Wideband surface impedance measurements in superconducting films," *IEEE Trans. Instrum. Meas.*, vol. 65, no. 5, pp. 1120–1129, 2016.